Volume 1 | Number 1 | Jan 2013 | Pages 1–100

Nanoscale

www.rsc.org/nanoscale

ROYAL SOCIETY OF CHEMISTRY

ROYAL SOCIETY OF CHEMISTRY

www.rsc.org/nanoscale

Nanoscale

A new synthesis of carbon encapsulated Fe₅C₂ nanoparticles for high-temperature Fischer-Tropsch synthesis

Seok Yong Hong,[a,b] Dong Hyun Chun,[a,b] Jung-Il Yang,[a] Heon Jung,[a] Ho-Tae Lee,[a] Sungjun Hong,[a] Sanha Jang,[a] Jung Tae Lim,[c] Chul Sung Kim,[c] and Ji Chan Park[a,b]*

Using a simple thermal treatment under CO flow, uniform micrometer-sized iron oxalate dihydrate cubes prepared by hydrothermal reaction were transformed into Fe₅C₂@C nanoparticles to form a mesoporous framework; the final structure was successfully applied to the high-temperature Fischer-Tropsch reaction and showed high activity (CO conversion=96%, FTY=1.5×10⁻⁴ mol_CO·g_Fe⁻¹·s⁻¹) and stability.

Fischer-Tropsch synthesis (FTS), normally performed using cobalt- and iron-based catalysts, has been a key technology for producing synthetic fuel from a mixture of carbon monoxide and hydrogen, generated from fossil resources such as coal, natural gas, and biomass.[1,2] However, the involved catalysts have been found to suffer from deactivation because of carbon deposition, particle agglomeration/sintering, and iron phase transformations during the high-temperature reaction.[3] To minimize the carbon deposits, α-Al₂O₃ has been used as a good support to increase dispersion of the iron.[4] Zhou et al. reported that the hierarchical structure of α-Al₂O₃, with high resistance against carbon deposits, showed better dispersion and immobilization properties for iron species than did those of commercial α-Al₂O₃.[5] However, when the iron oxide crystallite size is very small (sub-10 nm), the reduction/activation of iron oxide to active Fe₅C₂ phase on alumina supports, was rather more difficult than that on carbon supports because of strong interaction with the metal support.[6]

Carbon materials (e.g., activated carbon (AC), carbon nanofibers (CNFs), carbon nanotubes (CNTs), and graphene), have been used as catalyst supports in high-temperature Fischer-Tropsch synthesis (HT-FTS), because of their high specific surface area, chemical inertness, and controllable surface and pore structures.[7-11] Recently, new types of catalysts with carbon support have been developed

with enhanced activity and stability in FTS. For example, a "nanochannel reactor" system, which consists of an inner layer of Co nanoparticles and an outer layer of channel-like mesoporous carbon material (CMK-3), was suggested by Ha et al.[12] Yu et al. also reported the use of FeOₓ@C microspheres prepared by a simple hydrothermal reaction of glucose and iron nitrate, as a stable and selective catalyst for FTS.[13]

Over the past decade, core-shell and yolk-shell nanostructures, based on their intrinsic architecture, have been employed in various types of heterogeneous catalysis.[14,15] In particular, metal@silica core-shells and yolk-shells (metal = Ni, Pt, Pd, Au, Co, or others), generally prepared using the Stöber method, have shown their high thermal stability for high-temperature catalytic reactions.[16-18] It has also been found possible to synthesize metal@carbon core-shell nanostructures by various routes including catalytic decomposition of methane, plasma decomposition, controlled pyrolysis, and microwave arcing.[19-23] However, these synthetic routes are still complex and difficult, often yielding irregular products.

Recently, the simple thermal treatment of Prussian blue (Fe₄[Fe(CN)₆]₃) as a metal-organic framework (MOF) has been found to produce hierarchically structured Fe₂O₃ microboxes.[24] In a similar way, Santos et al. prepared highly active and stable Fe@C catalysts with high Fe load (25-38 wt%) using Fe-based MOF-mediated synthesis.[25] Although some studies on the preparation of Fe₅C₂ nanoparticles or Fe₅C₂/activated charcoal as active catalysts have been conducted,[26,27] to the best of our knowledge, there have been thus far no general synthetic schemes for Fe₅C₂@C catalyst structures, especially those containing active Hägg carbide (Fe₅C₂) nanoparticles. It is anticipated that pure Fe₅C₂ nanoparticles will
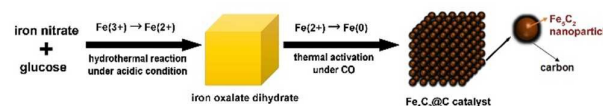
Scheme 1 Synthetic procedures for an Fe₅C₂@C catalyst.

a. Clean Fuel Laboratory, Korea Institute of Energy Research, 152, Gajeong-Ro, Daejeon, 305-343, Korea. E-mail: jcpark@kier.re.kr
b. Advanced Energy and Technology, University of Science and Technology, 217 Gajeong-Ro, Daejeon, 305-343, Korea.
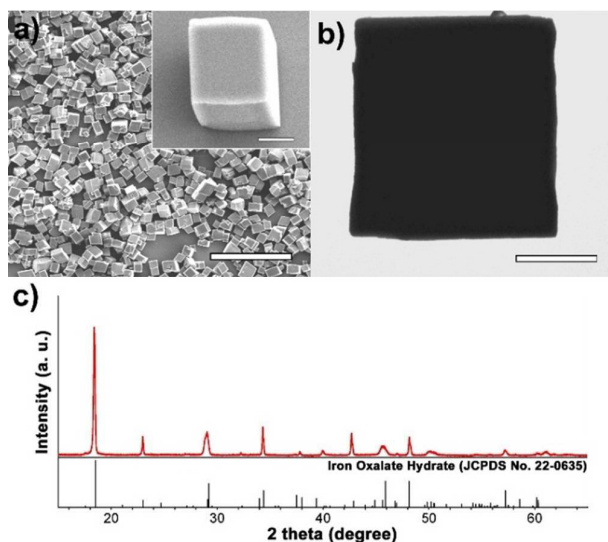c. Department of Physics, Kookmin University, Seoul, 136-702, Korea

Fig. 1 (a) SEM image, (b) TEM image, and (c) XRD spectrum of iron oxalate hydrate cubes. Inset of a) SEM image with a tilted angle of 40°. The bars represent 50 μm (a), 3 μm (inset of a), and 2 μm (b).

exhibit superior catalytic performance in FTS. In the present work, through the simple thermal treatment of iron oxalate dihydrate cubes under CO flow, we fabricated a three-dimensional Fe_5C_2@C catalyst holding single crystalline Fe_5C_2 nanoparticles of 10 nm diameter in graphitic carbon shells (1-2 nm) (**Scheme 1**).

First, cube-like iron oxalate dihydrate particles were obtained by hydrothermal reaction of aqueous Fe (III) solution with poly (vinyl pyrrolidone) (PVP) as a surfactant and glucose as a carbon source. Fe (III) solution was prepared by melting iron nitrate nonahydrate salt at 50 °C and injecting it into a hot surfactant solution containing PVP and glucose at 100 °C. The reaction mixture was refluxed for 1 h at the same temperature. As the reaction proceeded, the initially dark solution gradually turned yellow, indicating the formation of the iron (II) oxalate (FeC_2O_4) phase. During the reaction, the glucose was decomposed to oxalate ion ($C_2O_4^{2-}$) under the acidic condition of pH=0.9, derived from the Fe nitrate precursor used. Scanning electron microscopy (SEM) and transmission electron microscopy (TEM) images of the resultant iron oxalate dihydrate particles indicate uniform cubic shapes with an average edge size of 7.1±1.0 μm (**Fig. 1a-b**). In the X-ray diffraction (XRD) pattern, the micro-sized cubes are well-matched with those of iron oxalate dihydrate of orthorhombic phase (**Fig. 1c**, JCPDS no. 22-0635). The intense peak at $2\theta = 18.5°$ corresponds to the (202) plane of $FeC_2O_4 \cdot 2H_2O$. It should be possible to extend use of this synthetic route to prepare other iron-based alloy particles such as iron-nickel and iron-cobalt oxalate hydrates (**Fig. S1,** See Electronic Supplementary Information).

Next, the obtained micro-sized iron oxalate dihydrate cubes were decomposed to small iron carbide particles by thermal treatment at 350 °C under CO flow. During the reaction, the yellowish iron oxalate dihydrate powder changed to black, indicating the formation of the iron carbide phase. After the reaction, the initial iron oxalate dihydrate cubes were completely transformed to a mesoporous Fe_5C_2@C structure. In the SEM image, the resultant
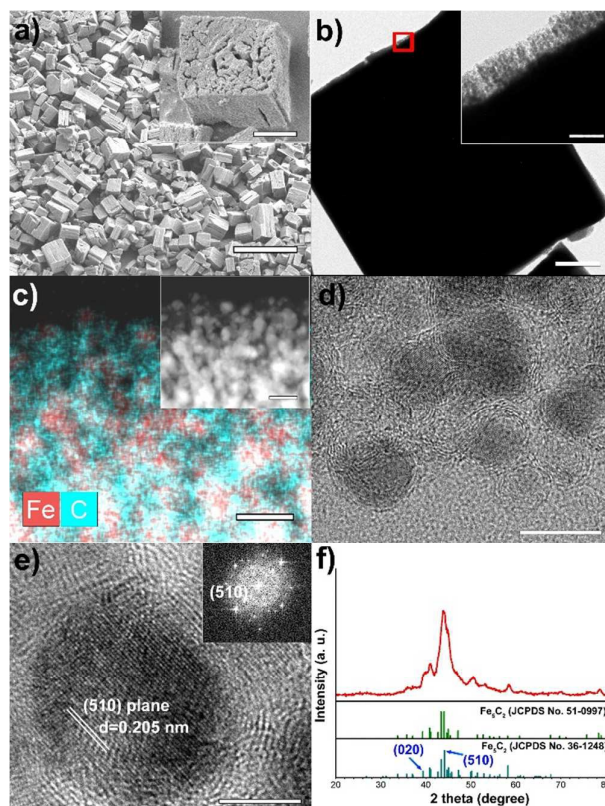

Fig. 2 (a) SEM and magnified SEM images (inset), (b) TEM and magnified TEM images (inset), (c) HAADF TEM image (inset) and scanning TEM image with elemental mapping of iron and carbon, (d-e) HRTEM images, (f) XRD spectrum of Fe_5C_2@C catalyst. The bars represent 20 μm (a), 2 μm (inset of a), 1 μm (b), 100 nm (inset of b), 20 nm (c and inset of c), 10 nm (d), and 5 nm (e).

Fe_5C_2@C catalyst also shows three-dimensional cubic structures (**Fig. 2a**). The large cubes obtained by thermal treatment were observed to be 4-5 μm in edge size, which is much shorter than the 7 μm typical of the original $FeC_2O_4 \cdot 2H_2O$. In the magnified SEM image, large crack-like pores in the single cube can clearly be observed (**inset of Fig. 2a**). The chemical reaction for the particle shrinking and pore generation, induced by spouting CO_2,[28] is proposed to be:

$$5FeC_2O_4 \cdot 2H_2O \text{ (s)} + 4CO \text{ (g)} \rightarrow Fe_5C_2 \text{ (s)} + 12CO_2 \text{ (g)} + 10H_2O \text{ (g)}$$
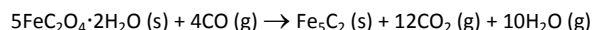
Simultaneously, the Boudouard reaction,[24] which forms gaseous carbon dioxide and solid graphitic carbon shells, occurred as follows:

$$2CO \text{ (g)} = CO_2 \text{ (g)} + C \text{ (s)}$$
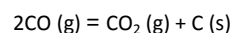
Based on these two reactions, the initial iron oxalate dihydrate particles were successfully transformed to mesoporous Fe_5C_2@C structures. In the TEM image, the micro-sized single particle shows its rectangular shape (**Fig. 2b**). The magnified TEM image of the red square in Figure 2b shows a cube's edge area, consisting of small particles and pores (**inset of Fig. 2b**). The high-angle annular dark-
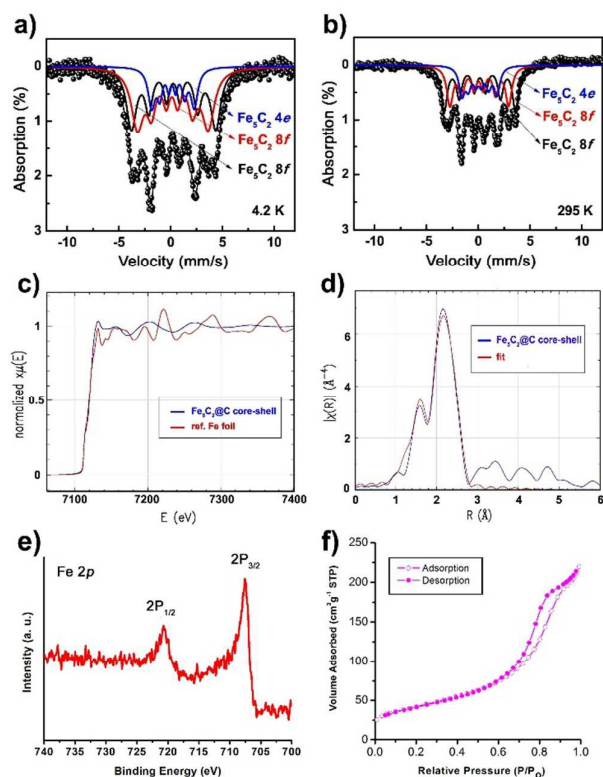
Nanoscale Accepted Manuscript

COMMUNICATION

Fig. 3 Mössbauer spectra at (a) 4.2 and (b) 295 K; (c) normalized Fe K-edge X-ray absorption spectrum, (d) Fe K-edge EXAFS spectrum, (e) XPS spectrum, and (f) N_2 adsorption–desorption isotherm of Fe_5C_2@C catalyst.

Fig. 4 CO conversion data for (a) Fe_5C_2@C catalyst, (b) conventional Fe/SBA-15 catalyst, and (c) hydrocarbon product selectivity graphs for Fe_5C_2@C catalyst in HT-FTS. The reaction tests were conducted at 320 ^{o}C, 15 bar, GHSV of 8.0 NL•g_{cat}^{-1}•h^{-1}, and an H_2:CO ratio of 1.

field scanning transmission electron microscopy (HAADF-STEM) image indicates relatively bright and dark areas (**inset of Fig. 2c**). The bright spots in the HADDF-STEM image primarily originate from heavy Fe atoms, whereas the dark spots are caused by light C atoms. In the elemental mapping of carbon (cyan colour) and iron (red colour), the presence of iron-rich sites; i.e., the presence of Fe_5C_2 particles, was confirmed (**Fig. 2c**). High-resolution TEM (HRTEM) analysis also revealed Fe_5C_2 nanoparticles encapsulated in graphitic carbon shells as well as in the pores among the particles (**Fig. 2d**). The inside particle size was observed to be 10.0 ± 1.3 nm for an average diameter (**Fig. S2**). The HRTEM image and the corresponding Fourier-Transform (FT) pattern show the single crystalline nature of the Hägg carbide particle. The lattice distance of 0.205 nm between neighbouring fringes corresponded to that of the (510) lattice spacing (0.205 nm) in monoclinic Fe_5C_2 (**Fig. 2e**). The presence of a large number of Fe_5C_2 (510) crystal facets can suppress methane formation and enhance carbon coupling, leading to high activity in HT-FTS.[30-31]

The XRD spectrum shows a broad and intense peak at $2\theta = 44^o$ that was found to match the two Hägg carbide phases (**Fig. 2f**, JCPDS no. 36-1248 and no. 51-0997). The very broad peak around $2\theta = 26^o$ could have originated from thin graphite layers (JCPDS no. 41-1487). Using the Debye–Scherrer equation, the average size of the Fe_5C_2 core is estimated to be 9.2 nm from the broadness of the (020) peak; this value is well-matched with the 10 nm value observed in the TEM images.
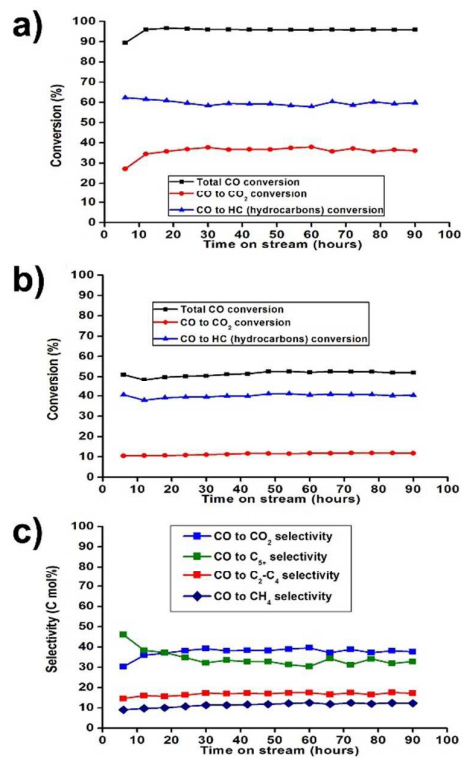
Using Mössbauer spectroscopy, it was possible to ascertain accurate values for the iron carbide species, and the distribution of the iron- based emergent materials (**Fig. 3a-b, Table S1**). The Mössbauer spectra obtained at 4.2 and 295 K show a superposition of the three-sextets of the Fe sites, corresponding to the spectrum of pure Fe_5C_2 crystallography sites without any other iron carbide phases (e.g., $Fe_{2.2}C$, Fe_2C, or Fe_3C). To check the oxidation state in the bulk form, and to determine the binding environment for Fe atoms within C molecules, X-ray absorption spectroscopy (XAS) was also conducted. In the X-ray absorption near-edge structure (XANES) region from one absorption edge to 7162 eV, an Fe pre-edge peak of the Fe_5C_2@C catalyst was observed at 7112 eV, which is well-matched with the peak of metallic Fe (**Fig. 3c**). The extended X-ray absorption fine structure (EXAFS) pattern of the Fe_5C_2@C catalyst shows the two major peaks of the first two coordination shells of Fe_5C_2, originating from Fe-C (1.6 Å) and Fe-Fe (2.2 Å) scattering (**Fig. 3d**). The core-level X-ray photoelectron spectroscopy (XPS) spectrum was measured to confirm the surface states of Fe in the Fe_5C_2@C core-shell structure (**Fig. 3e**). The XPS spectrum of the energy region of the Fe bands exhibits only one set of assigned sharp peaks from iron carbide (Fe(0)) at 707.6 eV and 720.7 eV, without other iron oxide species. Using inductively coupled plasma atomic emission spectroscopy (ICP-AES), the Fe load in the Fe_5C_2@C catalyst was measured and found to be 61 wt%. The N_2 sorption experiment at 77K for the Fe_5C_2@C catalyst exhibited type IV adsorption-desorption hysteresis (**Fig. 3f**). The Brunauer-Emmett-Teller (BET) surface area and the total pore volume were calculated

to be 152 $m^2 \cdot g^{-1}$ and 0.34 $cm^3 \cdot g^{-1}$, respectively. The low values of the BET surface area and pore volume were mainly attributed to the much higher Fe load (> 60 wt%) of the $Fe_5C_2@C$ catalyst, compared with the value of 20 wt% of conventional Fe-based supported catalysts. The pore size of the $Fe_5C_2@C$ catalyst was found to be 11 nm using the Barrett–Joyner–Halenda (BJH) method on the adsorption branch (**Fig. S3**).

Based on the unique morphology of many pores and robust carbon shells over active core particles, the $Fe_5C_2@C$ framework is very attractive for high-temperature catalysis. Here, we demonstrate using the HT-FTS reaction to verify the high activity and stability derived from pure Fe_5C_2 nanoparticles encapsulated in graphitic carbon shells. Until now, many mesoporous silica and carbon structures have been used as optimized support in preparing the active FT catalysts.[32,33] Therefore, the performance of the $Fe_5C_2@C$ catalyst was compared with the performance of conventional mesoporous catalysts, i.e., Fe/SBA-15 and Fe/activated carbon (Fe/AC), which were prepared using the incipient wetness method.[34]

First, we diluted the original $Fe_5C_2@C$ powder with activated charcoal in order to fix the Fe loading at 20 wt%, which is identical to the value used for conventional catalysts, and then ran the catalytic reaction. Prior to the FTS reaction, Fe/SBA-15 and Fe/AC were reduced in-situ under CO flow at 623 K for 4 h to allow sufficient activation of the initial iron oxide phases to the iron carbide phases. On the other hand, because the active Fe_5C_2 phase had already been generated during the catalyst preparation step before FTS reaction, the $Fe_5C_2@C$ catalyst was directly employed in HT-FTS without an extra in-situ activation process. The HT-FTS reaction tests were carried out at 15-20 bar, 320-340 °C, an H_2/CO ratio of 1, and high gas hourly space velocity (GHSV) conditions of 8.0-60.0 $NL \cdot g_{cat}^{-1} \cdot h^{-1}$ (**Table S2**). The CO conversion and selectivity of the catalysts were measured for 90 h by gas chromatography (GC) analysis of the outlet gasses. Liquid hydrocarbons were analysed by simulated distillation (SIMDIS).

The $Fe_5C_2@C$ catalyst showed a much higher total CO conversion of 96% at GHSV = 8.0 $NL \cdot g_{cat}^{-1} \cdot h^{-1}$, comparable to the conversion of 52% of the conventional Fe/SBA-15 (**Fig. 4a-b**). The catalyst activity is noted to be an iron-time-yield (FTY, the number of CO moles converted to hydrocarbons per gram of iron per second) over time-on-stream (TOS) (**Fig. S4**). For the $Fe_5C_2@C$ catalyst, the FTY value at 90 h was calculated and found to be 1.5×10^{-4} $mol_{CO} \cdot g_{Fe}^{-1} \cdot s^{-1}$, which is 1.5 times higher value than the activity (1.0×10^{-4} $mol_{CO} \cdot g_{Fe}^{-1} \cdot s^{-1}$) of Fe/SBA-15. Because of the complete formation of active Fe_5C_2 species and the prevention of particle sintering, it was possible to obtain high CO conversion and FT activity. In general, when FTS proceeds under higher GHSV, with harsher conditions of high reaction temperature and pressure, FTY values can increase dramatically even when using the same catalyst. Under the elevated reaction condition at 340 °C, 20 bar, and 60 $NL \cdot g_{cat}^{-1} \cdot h^{-1}$ in GHSV, the $Fe_5C_2@C$ catalyst also showed a very high FTY value of 5.2×10^{-4} $mol_{CO} \cdot g_{Fe}^{-1} \cdot s^{-1}$ at TOS= 90 h, which is similar to 4.9×10^{-4} $mol_{CO} \cdot g_{Fe}^{-1} \cdot s^{-1}$ at TOS= 4 h of the recently reported 25-Fe@C catalyst (**Fig. S5, Table S2**).[25]

In the selectivity data of the $Fe_5C_2@C$ catalyst, the selectivity of CO_2 (37.6%), CH_4 (12.3%), C_2-C_4 (17.2%), and C_{5+} (32.9%) were observed

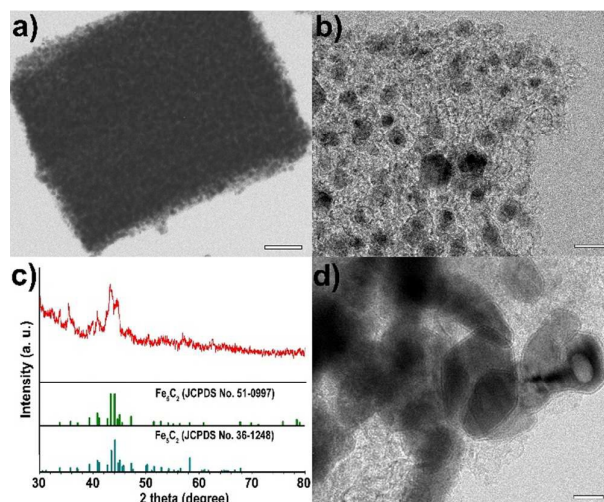**Fig. 5** (a) The TEM image, (b) HRTEM image, (c) XRD spectrum of the $Fe_5C_2@C$ catalyst recovered from the FT reaction over 90 h, and (d) TEM image of the recovered Fe/AC catalyst after reaction. The bars represent (a) 500 nm and (b, d) 20 nm.

at TOS 90 h (**Fig. 4c**). The total hydrocarbon (HC) product yields (grams of generated hydrocarbons per gram of iron per second) were measured after 90 h on stream of the reaction (**Fig. S6**). For the $Fe_5C_2@C$ catalyst, the total HC product yield (1.3×10^{-4} $g_{HC} \cdot g_{Fe}^{-1} \cdot s^{-1}$), calculated using the sum of the specific product yields, was 1.8 times higher than 7.3×10^{-5} $g_{HC} \cdot g_{Fe}^{-1} \cdot s^{-1}$ of Fe/SBA-15. The chain growth probability (α) of the hydrocarbons was calculated to be 0.786 using the Anderson-Schulz-Flory (ASF) chain growth mechanism (**Fig. S7**).[35]

After reaction for 90 h, the $Fe_5C_2@C$ catalyst still maintained its original cubic framework, consisting of small $Fe_5C_2@C$ nanoparticles (**Fig. 5a**); whereas the particles in Fe/AC catalyst were sintered to form large particles outside the carbon support (**Fig. 5d**). The low FT activity (0.7×10^{-5} $mol_{CO} \cdot g_{Fe}^{-1} \cdot s^{-1}$) of Fe/AC mainly originated from particle agglomeration during the HT-FTS reaction (**Table S2**). In the HRTEM image, the recovered $Fe_5C_2@C$ catalyst showed slightly larger Fe_5C_2 particles reflecting sharper peaks (**Fig. 5b**), but any significant phase transition from the original one was not observed (**Fig. 5c**).

In conclusion, a unique $Fe_5C_2@C$ catalyst holding highly active Fe_5C_2 nanoparticles of 10 nm size in graphitic carbon shells was prepared using a facile thermal treatment under CO flow of micrometer-sized iron oxalate dihydrate cubes. The carbon encapsulated Fe_5C_2 nanoparticles showed very high activity even without an extra in-situ activation step. It also showed good stability during high-temperature Fischer-Tropsch synthesis, because the mesoporous framework consists of only Fe_5C_2 cores (without other iron oxide species) and robust carbon shells. In addition, by introducing appropriate metal oxalate dihydrate cubes (e.g., metal= Ni, Co, Mo), it is anticipated that this approach could be extended to the preparation of other metal@carbon core-shell frameworks for catalysis of high-temperature reactions.

Notes and references

1   A. Y. Khodakov, W. Chu and P. Fongarland, *Chem. Rev.*, 2007, **107**, 1692.
2   Q. Zhang, J. Kang and Y. Wang, *ChemCatChem*, 2010, **2**, 1030.
3   E. de Smit and B. M. Weckhuysen, *Chem. Soc. Rev.*, 2008, **37**, 2758.
4   A. C. J. Koeken, H. M. T. Galvis, T. Davidian, M. Ruitenbeek and K. P. de Jong, *Angew. Chem. Int. Ed.*, 2012, **51**, 7190.
5   X. Zhou, J. Ji, D. Wang, X. Duan, G. Qian, D. Chen and X. Zhou, *Chem. Commun.*, 2015, **51**, 8853.
6   H. M. T. Galvis, J. H. Bitter, T. Davidian, M. Ruitenbeek, A. I. Dugulan and K. P. de Jong, *J. Am. Chem. Soc.*, 2012, **134**, 16207.
7   H. M. T. Galvis, J. H. Bitter, C. B. Khare, M. Ruitenbeek, A. I. Dugulan and K. P. de Jong, *Science*, 2012, **335**, 835.
8   W. Chen, Z. Fan, X. Pan and X. Bao, *J. Am. Chem. Soc.*, 2008, **130**, 9414.
9   S. O. Moussa, L. S. Panchakarala, M. Q. Ho and M. S. El-Shall, *ACS. Catal.*, 2014, **4**, 535.
10   K. Cheng, V. V. Ordomsky, M. Virginie, B. Legras, P. A. Chernavskii, V. O. Kazak, C. Cordier, S. Paul, Y. Wang and A. Y. Khodakov, *Appl. Catal. A: Gen.*, 2014, **488**, 66.
11   Y. Yang, K. Chiang and N. Burke, *Catal. Today*, 2011, 1**78**, 197.
12   K.-S. Ha, G. Kwak, K.-W. Jun, J. Hwang and J. Lee, *Chem. Commun.*, 2013, **49**, 5141.
13   G. Yu, B. Sun, Y. Pei, S. Xie, S. Yan, M. Qiao, K. Fan, X. Zhang and B. Zong, *J. Am. Chem. Soc.*, 2010, **132**, 935.
14   Y. Yin, R. M. Rioux, C. K. Erdonmez, S. Hughes, G. A. Somorjai and A. P. Alivisatos, *Science*, 2004, **304**, 711.
15   Q. Zhang, I. Lee, J. B. Joo, F. Zaera and Y. Yin, *Acc. Chem. Res.*, 2012, **46**, 1816.
16   J. C. Park and H. Song, *Nano Res.*, 2011, **4**, 33.
17   J. C. Park, J. U. Bang, J. Lee, C. H. Ko and H. Song, *J. Mater. Chem.*, 2010, **20**, 1239.
18   S. H. Joo, J. Y. Park, C.-K. Tsung, Y. Yamada, P. Yang and G. A. Somorjai, *Nat. Mater.*, 2009, **8**, 126.
19   S. K. Sengar, B. R. Mehta, R. Kumar and V. Singh, *Sci. Rep.* 2013, **3**, 2814.
20   S. C. Tsang, V. Caps, I. Paraskevas, D. Chadwick and D. Thompsett, *Angew. Chem. Int. Ed.*, 2004, **43**, 5645.
21   A.-H. Lu, W.-C. Li, N, Matoussevitch, B. Spliethoff, H. Bönnemann and F. Schüth, *Chem. Commun.*, 2005, **1**, 98.
22   G.-X. Zhu, X.-W. Wei and S. Jiang, *J. Mater. Chem.*, 2007, **17**, 2301.
23   Y.-L. Hsin, C.-F. Lin, Y.-C. Liang, K. C. Hwang, J.-C. Horng, J. A. Ho, C.-C. Lin and J. R. Hwu, *Adv. Funct. Mater.*, 2008, **18**, 2048.
24   L. Zhang, H. B. Wu, S. Madhavi, H. H. Hng and X. W. Lou, *J. Am. Chem. Soc.*, 2012, **134**, 17388.
25   V. P. Santos, T. A. Wezendonk, J. J. D. Jaén, A. I. Dugulan, M. A. Nasalevich, H.-U. Islam, A. Chojecki, S. Sartipi, X. Sun, A. A. Hakeem, A. C. J. Koeken, M. Ruitenbeek, T. Davidian, G. R. Meima, G. Sankar, F. Kapteijn, M. Makkee and J. Gascon, *Nat. Commun.*, 2015, **6**, 6451.
26   C. Yang, H. Zhao, Y. Hou and D. Ma, *J. Am. Chem. Soc.*, 2012, **134**, 15814.
27   J. C. Park, S. C. Yeo, D. H. Chun, J. T. Lim, J.-I. Yang, H.-T. Lee, S. Hong, H. M. Lee, C. S. Kim and H. Jung, *J. Mater. Chem. A*, 2014, **2**, 14371.
28   M. Hermanek, R. Zboril, M. Mashlan, L. Machala and O. Schneeweiss, *J. Mater. Chem.*, 2006, **16**, 1273.
29   W. Zhu, J. Ren, X. Gu, M. U. Azmat, G. Lu and Y. Wang, *Carbon*, 2011, **49**, 1462.
30   T. H. Pham, Y. Qi, J. Yang, X. Duan, G. Qian, X. Zhou, D. Chen and W. Yuan, ACS. Catal. 2015, **5**. 2203.
31   T. H. Pham. X. Duan, G. Qian, X. Zhou, D. Chen, J. Phys. Chem. C, 2014, **118**, 10170.
32   K. Cheng, M. Virginie, V. V. Ordomsky, C. Cordier, P. A. Chernavskii, M. I. Ivantsov and A. Y. Khodakov, *J. Catal.*, 2015, **328**, 139.
33   V. V. Ordomsky, B. Legras, K. Cheng, S. Paul and A. Y. Khodakov, *Catal. Sci. Technol.*, 2015, **5**, 1433.
34   A. J. Van Dillen, R. J.A.M. Terörde, D. J. Lensveld, J. W. Geus and K. P. de Jong, *J. Catal.*, 2003, **216**, 257.
35   I. Puskas and R. S. Hurlbut, *Catal. Today*, 2003, **84**, 99.

Nanoscale Accepted Manuscript

Nanoscale

Electronic Supplementary Information

A new synthesis of carbon encapsulated Fe_5C_2 nanoparticles for high-temperature Fischer-Tropsch synthesis

Seok Yong Hong, Dong Hyun Chun, Jung-Il Yang, Heon Jung, Ho-Tae Lee, Sungjun Hong, Sanha Jang, Jung Tae Lim, Chul Sung Kim, and Ji Chan Park*

Clean Fuel Laboratory, Korea Institute of Energy Research, Daejeon, Korea.

Advanced Energy and Technology, University of Science and Technology, Daejeon, Korea.

Department of Physics, Kookmin University, Seoul, 136-702, Korea

Experimental Section

Chemicals. Iron nitrate nonahydrate ($Fe(NO_3)_3 \cdot 9H_2O$, ACS reagent, $\geq 98\%$), nickel nitrate hexahydrate ($Ni(NO_3)_2 \cdot 6H_2O$, 99.999%), cobalt nitrate hexahydrate ($Co(NO_3)_2 \cdot 6H_2O$, ACS reagent, $\geq 98\%$), poly (vinyl pyrrolidone) (PVP, $M_w = 55,000$), D-(+)-glucose (ACS reagent), activated charcoal (-100 mesh particle size, powder), and glass beads (425-600 μm size) were purchased from Aldrich. Activated carbon (powder) was obtained from Strem Chemicals Inc. The chemicals were used as received without further purification.

Synthesis of iron oxalate hydrate cube. The mixture of PVP (8.3 g, 75 mmol) and glucose (9.0 g, 50 mmol) was dissolved in 50 mL of distilled water, and then slowly heated to 100 °C for 20 min under inert condition. After that, $Fe(NO_3)_3 \cdot 9H_2O$ (10.1 g, 25 mmol), molten at 323 K, was injected into the hot PVP-glucose mixture solution at 373 K; the mixture solution was refluxed for 1 h at the same temperature. After 1 h, the colloidal dispersion was cooled to room temperature, and separated by centrifugation at 8,000 rpm for 10 min. Finally, the precipitates were washed with distilled water and ethanol several times with centrifugation at 8,000 rpm for 10 min; precipitates were dried in an oven at 333 K overnight to yield a yellowish powder.

Synthesis of iron-nickel oxalate hydrate and iron-cobalt oxalate hydrate particles. For the synthesis of nickel-iron oxalate hydrate particles, the mixture of PVP (8.3 g, 75 mmol) and glucose (9.0 g, 50 mmol) was dissolved in 50 mL of distilled water, and then slowly heated to 100 °C for 20 min under inert condition. After that, the mixed solution of $Fe(NO_3)_3 \cdot 9H_2O$ (5.1 g, 12.5 mmol) and $Ni(NO_3)_2 \cdot 6H_2O$ (3.6 g, 12.5 mmol), molten at 323 K, was injected into the hot PVP-glucose mixture solution at 373 K; the mixture solution was refluxed for 1 h at the same

temperature. After 1 h, the colloidal dispersion was cooled to room temperature, and separated by centrifugation at 8,000 rpm for 10 min. Finally, the precipitates were washed with distilled water and ethanol several times by centrifugation with 8,000 rpm for 10 min; precipitates were dried in an oven at 333 K. To prepare the iron-cobalt oxalate hydrate particles, $Co(NO_3)_2 \cdot 6H_2O$ (3.6 g, 12.5 mmol) was employed with $Fe(NO_3)_3 \cdot 9H_2O$ (5.1 g, 12.5 mmol). The procedures and conditions were identical to those used in the synthesis of iron-nickel oxalate hydrate particles.

Synthesis of Fe_5C_2@C catalyst. The iron oxalate hydrate powders (0.5 g) were transferred to an alumina boat in a tube-type furnace, and then heated very slowly, with a ramping rate of 0.15 K·min^{-1}, and activated to iron carbide phase at 623 K under a CO flow of 200 mL·min^{-1}. The sample was then thermally treated at the same temperature for 4 h under a continuous flow of CO.

Preparation of Fe/SBA-15 and Fe/AC catalysts. Mesoporous silica support SBA-15 was prepared using the hydrothermal reaction reported elsewhere. Next, using the incipient wetness method, $Fe(NO_3)_3 \cdot 9H_2O$ (1.8 g) dissolved in ethanol (5mL) was used to saturate calcined SBA-15 powders (1.0 g). Then, the resulting powder was dried in an oven at 373 K for 24 h and calcined under an N_2 flow of 200 mL·min^{-1} at 673 K for 4 h. This sample was designated Fe/SBA-15. For the preparation of Fe/AC catalyst, all procedures were identical to the synthesis of Fe/SBA-15, except for the use of activated carbon powders (1.0 g) as support.

High-temperature Fischer-Tropsch synthesis. Fischer-Tropsch (FT) reactions were carried out in a fixed-bed stainless steel reactor with inner diameter of 5 mm and length of 180 mm. The Fe loading content of the Fe_5C_2@C catalyst was adjusted to 20 wt% for comparison with those of Fe/SBA-15. The prepared catalyst (0.3 g) was diluted with glass beads (3.5 g) for prevention of hot-spot generation and then placed in the fixed-bed reactor. Prior to the reaction, in the case of the Fe/SBA-15 and Fe/AC samples, in-situ activation was additionally conducted under a CO flow of 40 mL·min^{-1} at 623 K for 4h. Then, the reaction was performed at 593 K and 15 bar for 90 h using a mixture gas (H_2/CO=1.0, GHSV=8.0 NL·g_{cat}^{-1}·h^{-1}). The flow rates of the outlet gases were measured using a wet-gas flowmeter (Shinagawa Corp.); gases were analysed using an online gas chromatograph (Agilent, 3000A Micro-GC) equipped with molecular sieve and plot Q columns. After 90 h of Fischer-Tropsch synthesis, the solid hydrocarbon products and water were collected in a cold trap at 273 K. The compositions of the wax and the liquid oil were analysed by means of an offline GC (Agilent 6890 N) using a simulated distillation method (ASTM D2887). The total and specific product yields for each sample were obtained via gas chromatography (GC) analysis of the gaseous products (C_1–C_4), and simulated distillation (SIMDIS) analysis of the isolated solid (wax) and the liquid (oil) products.

Characterization. SEM images of the samples were obtained using a Hitachi S-4800 operated at 5 kV. High resolution transmission electron microscopy (TEM) analysis was performed using a Tecnai TF30 ST and a Titan Double Cs corrected TEM (Titan cubed G2 60-300). Energy-dispersive X-ray spectroscopy (EDS) elemental mapping data were collected using a higher efficiency detection system (Super-X detector). High power powder-XRD (Rigaku D/MAX-2500, 18 kW) was also used for the analysis. XPS studies were carried out using a Sigma Probe (Thermo VG Scientific, Inc.) with a micro-focused monochromator X-ray source. The sample for XPS was prepared by placing a few drops of the colloidal solution on small pieces (5 mm × 5 mm) of gold wafer. The Fe X-ray absorption spectrum (XAS) was recorded on Beam-line 6D of the Pohang Accelerator Laboratory (PAL). The Mössbauer spectrum was obtained with a fixed absorber and a moving source. A Mössbauer spectrometer of the electromechanical type, with a 50 mCi ^{57}Co source in a rhodium matrix, was used in constant-acceleration mode. N_2-sorption isotherms were measured at 77 K with a Tristar II 3020 surface area analyser. Before measurement, the sample was degassed at 300 °C for 4 h under N_2 flow.
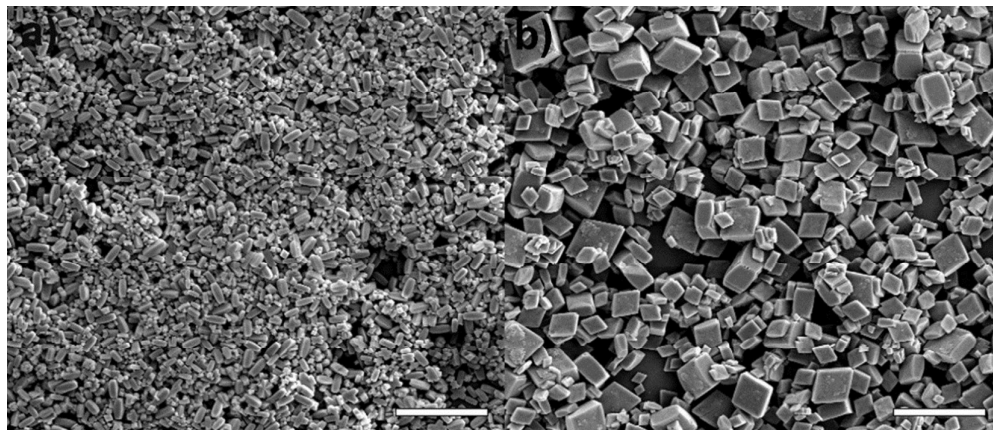
Nanoscale Accepted Manuscript

Figure S1. SEM images of (a) iron-nickel oxalate hydrate and (b) iron-cobalt oxalate hydrate particles. All bars represent 20 μm.
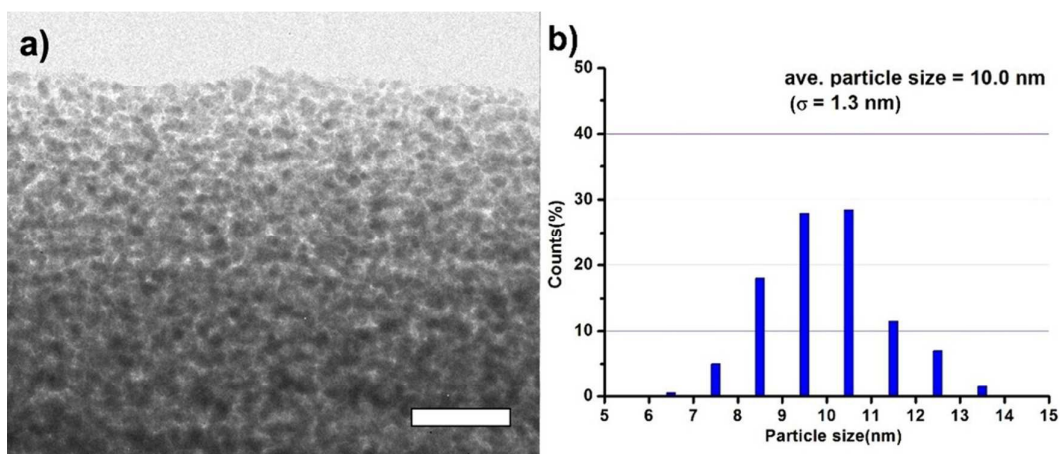

Figure S2. TEM image and particle size distribution histogram of Fe_5C_2 nanoparticles encapsulated in carbon shells. More than 200 particles were counted. The bar (a) represents 100 nm.
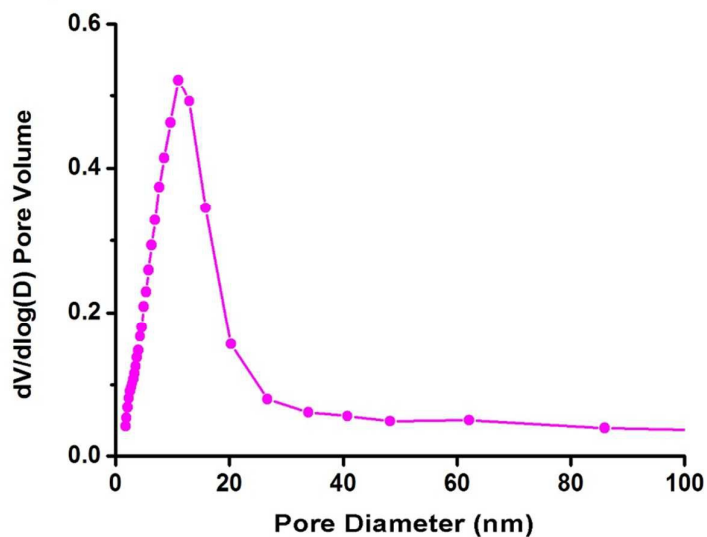
Figure S3. Pore size distribution diagram calculated from the adsorption branch of Fe_5C_2@C catalyst.
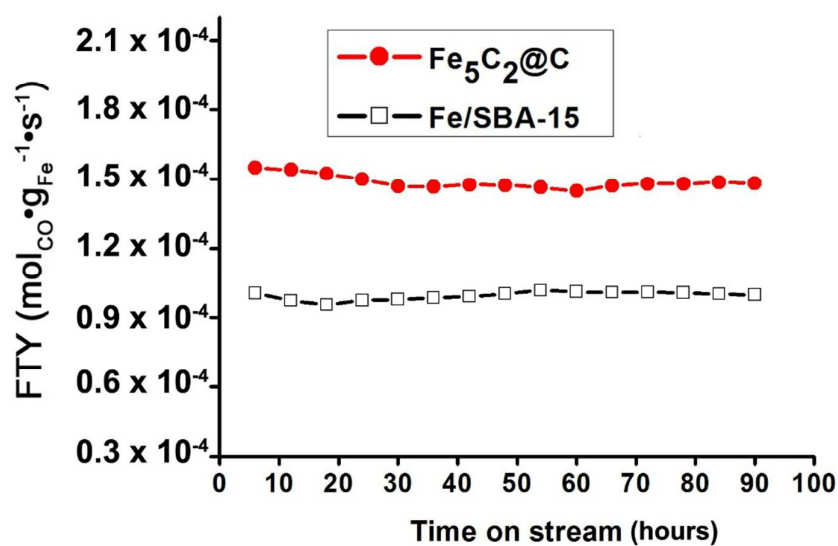

Figure S4. Catalytic performance of Fe_5C_2@C and Fe/SBA-15 catalysts for HT-FTS. The reaction tests were conducted at 320 ^{o}C, 15 bar, GHSV of 8.0 NL·g_{cat}^{-1}·h^{-1}, and an H_2:CO ratio of 1.
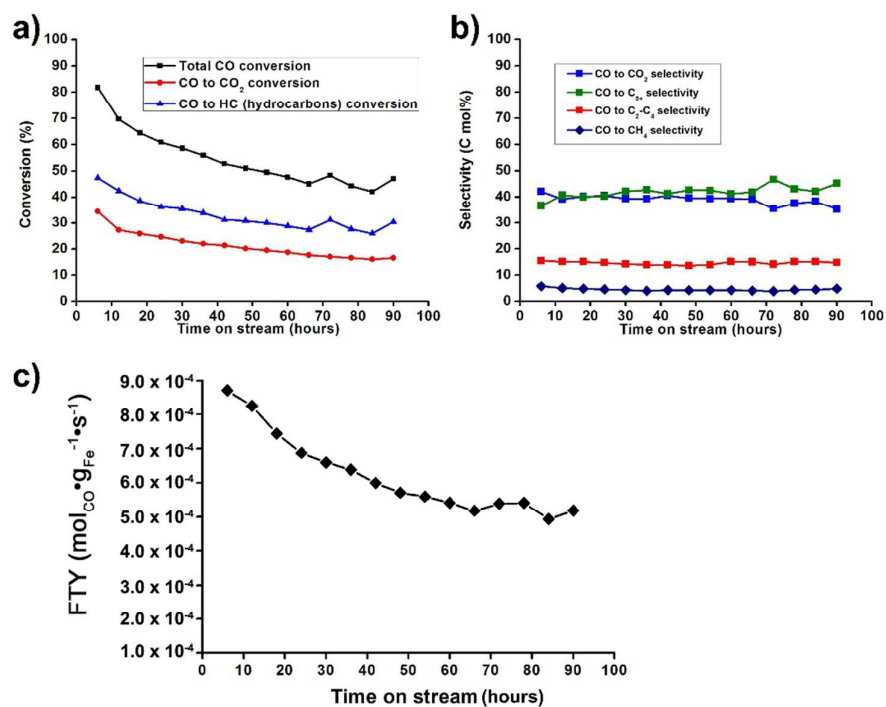
Figure S5. (a) CO conversion, (b) hydrocarbon product selectivity data, and (c) FT activity of $Fe_5C_2@C$ catalyst under the harsh HT-FTS reaction at 340 ^{o}C, 20 bar, GHSV of 60.0 $NL \cdot g_{cat}^{-1} \cdot h^{-1}$, and an H_2:CO ratio of 1.

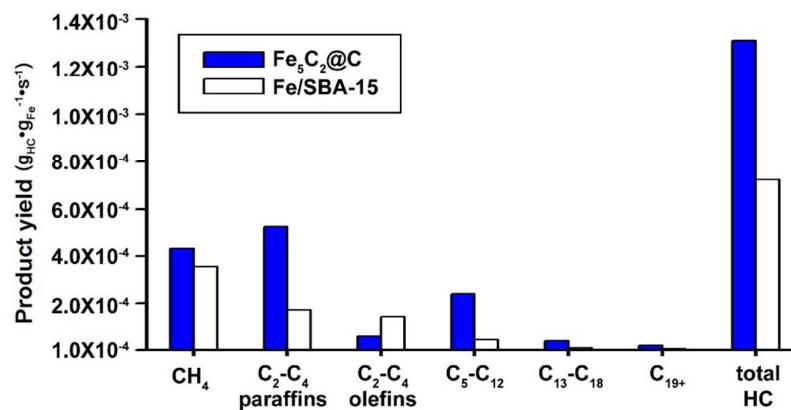**Figure S6.** Hydrocarbon product yields of $Fe_5C_2@C$ and Fe/SBA-15 catalysts in HT-FTS. The reaction tests were conducted at 320 ^{o}C, 15 bar, GHSV of 8.0 $NL \cdot g_{cat}^{-1} \cdot h^{-1}$, and an H_2:CO ratio of 1.
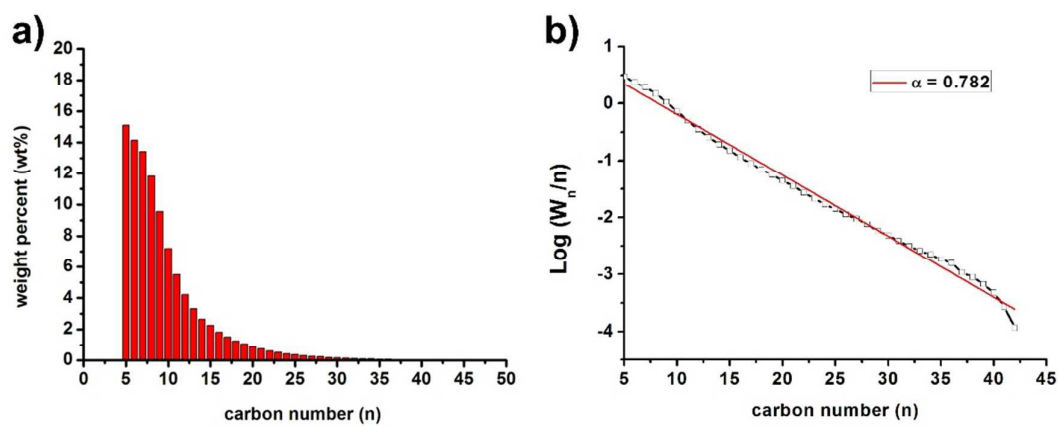
Figure S7. (a) C_{5+} liquid hydrocarbon product distribution and (b) ASF plot and chain growth probability of Fe_5C_2@C catalyst.

Table S1. Mössbauer parameters of the Fe_5C_2@C catalyst.

Temperature (K)		site		
		Fe_5C_2		
		I (8*f*)	II (8*f*)	III (4*e*)
295 K	H_{hf}(kOe)	213.77	176.28	105.31
	δ (mm/s)	0.15	0.06	0.07
	E_Q (mm/s)	0.00	0.04	0.05
	Area (%)	39.93	36.18	23.89
4.2 K	H_{hf}(kOe)	253.36	212.59	127.98
	δ (mm/s)	0.26	0.16	0.19
	E_Q (mm/s)	0.02	0.05	0.04
	Area (%)	37.81	44.90	17.29

H_{hf}: hyperfine magnetic field; δ: isomer shift (all the isomer shifts are referred to α-Fe at 295K); E_Q: quadrupole shift.

Table S2. Comparison of the CO conversion and FTS activity of $Fe_5C_2@C$ catalyst with those found in the literature for Fe supported catalysts in high-temperature FTS reactions.

Catalyst	GHSV ($NL \cdot g_{cat}^{-1} \cdot h^{-1}$)	Total CO conv. (%)	FTY ($mol_{CO} \cdot g_{Fe}^{-1} \cdot s^{-1}$)	Ref.
$Fe_5C_2@C$ catalyst diluted with activated charcoal (Fe: 20wt%)	8.0	96	1.5×10^{-4}	This work[a]
	12.0	84	2.0×10^{-4}	This work[a]
	16.0	68	2.2×10^{-4}	This work[a]
	60.0	47	5.2×10^{-4}	This work[c]
Fe/SBA-15 (Fe: 20 wt%)	8.0	52	1.0×10^{-4}	This work[a]
Fe/AC (Fe: 20wt%)	8.0	4.9	0.7×10^{-5}	This work[a]
K-doped Fe_5C_2/activated charcoal (Fe: 20wt%)	8.0	94	1.5×10^{-4}	1)[a]
10FeSi50 (Fe: 10 wt%)	16.2	33.8	2.0×10^{-4}	2)[b]
Fe@C (Fe: 25 wt%)	60.0	59	4.9×10^{-4}	3)[c]
$Fe_{15}Mn_5$/graphene (Fe: 15 wt%)	2.5	92	1.5×10^{-4}	4)[d]
Fe/CNT (Fe: 10 wt%)	16.2	85	4.7×10^{-4}	5)[e]
Fe/CNF (Fe: 12 wt%)	1.5	88	3.0×10^{-5}	6)[f]
Fe-Cu-K-SiO_2 (Fe: 32 wt%)	1.5	79	1.1×10^{-5}	
Fe/α-Al_2O_3 (Fe: 6 wt%)	1.5	77	8.5×10^{-5}	

Catalytic tests were carried out at [a]T = 320°C, P = 15 bar, H_2/CO ratio=1, [b]T = 300°C, P = 20 bar, H_2/CO ratio=2.1 [c]T = 340°C, P = 20 bar, H_2/CO ratio=1, [d]T = 325°C, P = 15 bar, H_2/CO ratio=2, [e]T = 300°C, P = 20 bar, H_2/CO ratio=2, [f]T = 340°C, P = 20 bar, H_2/CO ratio=1.

References:

1) J. C. Park, S. C. Yeo, D. H. Chun, J. T. Lim, J.-I. Yang, H.-T. Lee, S. Hong, H. M. Lee, C. S. Kim and H. Jung, *J. Mater. Chem. A*, 2014, **2**, 14371.

2) K. Cheng, M. Virginie, V. V. Ordomsky, C. Cordier, P. A. Chernavskii, M. I. Ivantsov and A. Y. Khodakov, *J. Catal.*, 2015, **328**, 139.

3) V. P. Santos, T. A. Wezendonk, J. J. D. Jaén, A. I. Dugulan, M. A. Nasalevich, H.-U. Islam, A. Chojecki, S. Sartipi, X. Sun, A. A. Hakeem, A. C.J. Koeken, M. Ruitenbeek, T. Davidian, G. R. Meima, G. Sankar, F. Kapteijn, M. Makkee and J. Gascon, *Nat. Commun.*, 2015, **6**, 6451.

4) S. O. Moussa, L. S. Panchakarla, M. Q. Ho and M. S. El-Shall, *ACS Catal.* 2014, **4**, 535.

5) V. V. Ordomsky, B. Legras, K. Cheng, S. Paul and A. Y. Khodakov, *Catal. Sci. Technol.*, 2015, **5**, 1433.

6) H. M. T. Galvis, J. H. Bitter, C. B. Khare, M. Ruitenbeek, A. I. Dugulan and K. P. de Jong, *Science*, 2012, **335**, 835.

Graphical Abstract

A novel $Fe_5C_2@C$ catalyst that bears small iron carbide particles with diameters of ~10 nm inside graphitic carbon shells, was prepared by simple thermal treatment of iron oxalate dihydrate cubes under CO flow; then was employed in high-temperature Fischer-Tropsch synthesis. The new catalyst exhibited high activity and exceptinal stability.